

The spontaneous elastoresistivity coefficient within the nematic ordered phase of iron pnictides

Joshua Sanchez¹, Paul Malinowski¹, Joshua Mutch¹, Jian Liu², J-W. Kim³, Philip J Ryan^{3,4}, Jiun-Haw Chu^{1,*}

Affiliation:

¹ Department of Physics, University of Washington, Seattle, Washington 98195, USA.

² Department of Physics, University of Tennessee, Knoxville, Tennessee 37996, USA.

³ Advanced Photon Source, Argonne National Laboratories, Lemont, Illinois 60439, USA.

⁴ School of Physical Sciences, Dublin City University, Dublin 9, Ireland.

*Correspondence to: jhchu@uw.edu (J.-H.C)

Key Words: electronic nematicity, iron-based superconductors, unconventional superconductivity, quantum critical point

Abstract:

When a symmetry is spontaneously broken in solids, a new transport coefficient emerges. A famous example is the anomalous Hall coefficient associated with broken time reversal symmetry. Here we present a measurement of the analogous transport coefficient in solids with broken rotational symmetry, the spontaneous elastoresistivity coefficient, defined as the ratio of the spontaneous resistivity anisotropy to the spontaneous structural distortion. In the iron pnictides, the measured spontaneous elastoresistivity coefficient coincides with the value of the normal elastoresistivity attained at the critical temperature of the nematic phase transition, which in a Landau free energy framework implies that the resistivity anisotropy remains a valid proxy of nematicity above and below the transition. Building on this equality, we find a nearly four-fold enhancement of the spontaneous elastoresistivity coefficient with doping towards optimal superconductivity. Our result reveals a clear sign of quantum critical enhancement of the coupling between nematicity and conduction electrons.

Introduction

Electronic nematicity refers to a spontaneous rotational symmetry breaking phase in solids driven by electronic correlations¹. Due to the finite electron-lattice coupling, electronic nematicity is always accompanied by a structural phase transition. From a symmetry point of view there is no distinction between a proper ferro-elastic transition and a nematically-driven structural transition. Nevertheless, a method to distinguish these two is the measurement of the elastoresistivity coefficient, which is the ratio of induced resistivity anisotropy to the externally applied anisotropic strain in the same symmetry channel as the nematic ordering². Above the phase transition, the elastoresistivity coefficient $2m_{66}$ is proportional to the B_{2g} nematic susceptibility, the divergence of which is a direct indicator of the electronically-driven instability. In numerous families of iron-based superconductors, $2m_{66}$ follows a Curie-Weiss temperature dependence over a large temperature and doping range, which established that the structural transition is electronically driven and revealed the prevalence of large nematic fluctuations at temperatures well *above* the phase transition²⁻⁴.

The proportional relationship between $2m_{66}$ and the B_{2g} nematic susceptibility originates from symmetry considerations. In the tetragonal point group the resistivity anisotropy $\eta = \frac{\rho_{xx} - \rho_{yy}}{\rho_{xx} + \rho_{yy}}$ and the Ising nematic order parameter ψ belong to the same irreducible representation, hence they are linearly proportional to each other in the infinitesimal limit ($\eta = k \psi$)⁵. This symmetry consideration has often been adopted as the argument to treat the resistivity anisotropy as a proxy of the nematic order parameter itself. Nevertheless, resistivity is not a thermodynamic variable and it depends on extrinsic properties such as disorder. While the perfect Curie-Weiss temperature dependence of $2m_{66}$ implicitly confirms that the proportional constant k is independent of temperature above the phase transition, it is still unclear whether the constant k is also invariant below the phase transition, especially when the order parameter grows beyond the infinitesimal limit.

Scrutinizing the relationship between resistivity anisotropy and nematicity is also critical to the understanding of superconducting pairing in iron-based materials. Optimal T_C is found in the vicinity of a fully suppressed nematic phase for most families of iron-based high-temperature superconductors. $2m_{66}$ has been shown to diverge towards zero temperature at the optimal doping in several families of materials, suggesting that the superconducting pairing may be enhanced by nematic quantum critical fluctuations^{2,4}. The conduction electrons that participate in pairing are ultimately the same electrons that give rise to the resistivity anisotropy, and so the constant k that quantifies the coupling of conduction electrons to nematicity also encodes the coupling to nematic fluctuations that forms the pairing glue.

Here we introduce a transport coefficient that directly measures the coupling of nematicity to conduction electrons, the *spontaneous* elastoresistivity coefficient, m_S , defined as the ratio of the spontaneous resistivity anisotropy to the spontaneous structural distortion below a phase transition. Whereas $2m_{66}$ measures the linear response due to the externally applied strain, m_S plays the same role as the anomalous Hall coefficient in a ferromagnet, which measures the coupling between conduction electrons and a $q = 0$ thermodynamic order parameter. Since m_S is defined within the broken symmetry phase, its zero-temperature limit reflects the ground state properties. For example, the doping dependence of m_S near the putative quantum critical point may reveal the transport anomaly in the broken symmetry side of the phase diagram, a region that has been rarely explored in the past^{6,7}

In this work, we introduce a method that precisely determines the spontaneous elastoresistivity coefficient by combining resistivity and x-ray diffraction measurement with in-situ tunable uniaxial stress. We show that the spontaneous elastoresistivity coefficient in the underdoped iron pnictide is a temperature independent quantity with a value equal to the value of $2m_{66}$ at the nematic transition temperature T_S . In the framework of the Landau free energy model, this equality is a direct confirmation that the proportional constant k is invariant across the phase transition. This equality also leads to an important consequence: in Figure 1, we show the values of $2m_{66}$ at the nematic transition temperature

T_S across the underdoped side of the Co-doping phase diagram. The evolution towards optimal superconductivity coincides with a nearly fourfold enhancement of the value of $2m_{66}(T_S)$, which suggests that the spontaneous elastoresistivity also increases by nearly fourfold near the optimal doping. Our study reveals a new aspect of metallic quantum criticality with implications to high-Tc superconductivity, namely that the coupling between static order and conducting electrons is enhanced as the quantum critical point is approached from the ordered side.

Precision Detwinning of Orthorhombic Domains

The main experimental challenge for a precise determination of the spontaneous elastoresistivity coefficient is the presence of orthorhombic twin domains, which cause transport measurements to average over the resistivities of the domains. Previous experiments detwinned samples using constant uniaxial stress via a clamp or constant uniaxial strain via a horseshoe device⁸⁻¹⁴, which revealed large transport anisotropies in the ordered state maintained down to the superconducting transition or base temperature. However, the large stresses induced by these devices inevitably result in additional lattice distortions, especially in the neighborhood of the structural transition where the elastic modulus softens¹⁵⁻¹⁷, obscuring the distinction between the spontaneous elastoresistivity coefficient (m_s) and the additional strain-induced resistivity anisotropy measured by the normal elastoresistivity coefficient ($2m_{66}$). More recently, the spontaneous resistivity anisotropy has been measured by the quantum gas imaging technique¹⁸. Another attempt to get around this issue is a pioneering work by Tanatar et al⁹, in which the resistivity of an FeSe sample was measured in two tensile strain states within the nematic phase. The resistivity anisotropy was then estimated by linear extrapolation. The validity of this method relies on two assumption: the strain measured from the detwin device is a true measure of the actual lattice distortion of the crystal, and the elastoresistivity is a linear function of strain. As we shall discuss below, neither of these assumptions holds near the phase transition.

We overcome these challenges by developing a new experimental platform that combines x-ray diffraction (XRD) and electrical transport with *in-situ* uniaxial stress tunability (Fig. 2a). This platform allows us to measure the lattice constants, orthorhombic twin domain populations, and electrical resistivity simultaneously while the uniaxial stress is continuously tuned. Using this platform, we detwin a sample of $x = 0.04$ underdoped $Ba(Fe_{1-x}Co_x)_2As_2$ and extract the spontaneous resistivity anisotropy ($\eta_0 = \frac{\rho_a - \rho_b}{\rho_a + \rho_b}$) and the zero-stress structural orthorhombicity ($\epsilon_0 = \frac{a-b}{a+b}$) within the nematic phase. The sample we use in this work is located in the underdoped side of the phase diagram with $T_S = 74K$, $T_N = 64K$ and $T_C = 74K$ (Fig. 1). We focus on the 10K range below T_S but above T_N because the long-range antiferromagnetic order reconstructs the Fermi surface and induces additional resistivity anisotropy effects^{19–22}. The key to this experiment is a uniaxial strain device²³ fully integrated with the beamline 6-ID-B, at the Advanced Photon Source (Fig. 2a) (see Methods). The lattice constants along the $[1\ 1\ 0]_T$, $[-1\ 1\ 0]_T$ and $[0\ 0\ 1]_T$ directions of the orthorhombic unit cell are determined from measuring the $(2\ 2\ 12)_T$, $(-1\ 1\ 14)_T$ and $(0\ 0\ 14)_T$ reflections in the tetragonal basis. The sample is oriented such that applied strain can detwin the sample and enhance the orthorhombicity. The nominal strain is defined as $\epsilon_{xx}^{nom} = \frac{\Delta L}{L_0}$, where L_0 is the size of the gap between two titanium plates on which the sample was glued with Stycast epoxy. The displacement ΔL was determined from a capacitance strain gauge. The four-wire electrical contact geometry enables the simultaneous resistance measurements along the strain axis.

Upon cooling the sample below 74K, the single peak of the $(2\ 2\ 12)_T$ reflection splits into two peaks corresponding to the a_A and b_B orthorhombic lattice constants of the A and B domains, respectively, indicating the formation of nematic twin domains (Fig. 2a-b). Figure 2c-f shows detwinning results for a representative temperature 8K below T_S . The peak positions and intensities (I_A and I_B) are shown in Figure 2c. The relative volume fraction of the A domain is determined as $D_A(\%) = \left(\frac{I_A}{I_A + I_B}\right) \times 100$, which varies smoothly with applied stress between 0% and 100% i.e. between the B and

A monodomains (Fig. 2e, right). While the sample is mostly detwinned over a relatively small strain range, the last 10% volume fraction of the minor domain appears to persist up to large strain values. Strain homogeneity is confirmed by a nearly-constant Bragg peak width throughout the nominal strain range (Fig. 2d). A video of the XRD detwinning data is available online.

The B_{2g} orthorhombicity within a domain is defined using lattice constants along both the $[1\ 1\ 0]_T$ and $[-1\ 1\ 0]_T$ directions as $\varepsilon = \frac{\alpha_A - b_A}{\alpha_A + b_A}, \frac{\alpha_B - b_B}{\alpha_B + b_B}$ under tension and compression, respectively. A precise measurement of the spontaneous orthorhombicity ε_0 within the nematic phase near zero nominal strain can be made using the split $(2\ 2\ 12)_T$ reflection as is often done for a freestanding crystal²⁴, with $\varepsilon_0 = \frac{\alpha_A - b_B}{\alpha_A + b_B}$ (Fig. 2c). We observe that ε_0 is nearly constant for D_A values between 10% and 90%, leading us to define this nominal strain range as the twin domain region (Fig. 2f, between grey bars). For larger nominal strains, the crystal is mostly detwinned to a monodomain, and the induced orthorhombicity increases dramatically with increasing tensile or compressive strain. Uniaxial stress then appears to be unable to remove the last 10% of the minor domain without changing the lattice constants of the major domain. Therefore, we find that we can mostly, but not fully, detwin the sample without inducing additional lattice distortions, which warrants consideration for the design and interpretation of future experiments involving the application of uniaxial stress to detwin orthorhombic domains.

The spontaneous resistivity anisotropy η_0 results from the resistivities of the distortion-free orthorhombic domain, ρ_a and ρ_b . Under large stress, the resistivity anisotropy is rapidly enhanced due to the elasto-resistance effect of the monodomain orthorhombic crystal. In the low-stress twin domain region, the orthorhombicity is nearly constant and so we ascribe changes of resistivity to biasing the domain populations and not to elasto-resistance effects. Due to the network of twin domains running at 45° to the length of the sample²⁵, the current takes nontrivial paths, with a preference for the lower-resistivity A domain, and so ρ_{xx} has a nonlinear response to D_A (Fig. 3a). Since the direct measurement of resistivity of a fully-detwinned zero-stress monodomain sample is not possible due to the persistence of the minor

domain, we determine η_0 at each temperature from the resistivities at the edges between the twin and monodomain regions, with $\rho_a = \rho_{xx}(D_A = 90\%)$ and $\rho_b = \rho_{xx}(D_A = 10\%)$ (Fig. 3b filled circles). Alternative choices within the twin domain region ($D_A = 15\%/85\%$) and in the elastoresistive strain range ($D_A = 5\%/95\%$) provide an under/over estimate of η_0 (grey/open circles).

The spontaneous resistivity anisotropy η_0 and the spontaneous orthorhombicity ε_0 are well fitted by $(T_s - T)^{\frac{1}{2}}$ (Fig. 3c-d). From the shared temperature dependence, we find that the ratio $m_s = \frac{\eta_0}{\varepsilon_0}$, i.e. the spontaneous elastoresistivity coefficient, has a temperature-independent value of $m_s \cong 155$ (135-195 for under/overestimate). The large value of m_s is consistent with previous uniaxial stress detwinned measurements, which revealed a resistivity anisotropy orders of magnitude larger than the orthorhombicity. Intriguingly, while the resistivity anisotropy is expected by symmetry to be linearly proportional to the primary nematic order parameter ψ in the infinitesimal limit ($\eta = k \psi$), the clear mean-field behavior of η_0 gives strong evidence that this linear relation is valid within the nematic phase even for large values of the order parameter (40% of the $T = 0K$ saturated value)²⁶, with a temperature independent proportionality constant k .

To gain more insight into the physical interpretation of m_s , we examine the Landau free energy that describes a nematic phase transition with a bilinear coupling to the lattice²⁷:

$$F = \frac{a_0(T - T^*)}{2} \psi^2 + \frac{b}{4} \psi^4 + \frac{C_{66,0}}{2} \varepsilon^2 - \lambda \psi \varepsilon$$

Here, T^* is the bare nematic transition temperature and $C_{66,0}$ is the bare elastic shear modulus^{15,16,28}, i.e. the elastic modulus of the crystal if there is no coupling to the nematicity. The B_{2g} orthorhombicity ε is linearly coupled to the nematic order parameter ψ via the nematic-elastic coupling term $\lambda \psi \varepsilon$. In the language of pseudoproper ferroelastic transitions, ψ is the primary order parameter and ε is the secondary order parameter. Within the nematic phase and in the absence of applied stress, the nematic order parameter develops with a mean-field temperature dependence as $\psi_0 \propto (T_s - T)^{\frac{1}{2}}$ which drives

the linearly-proportional spontaneous orthorhombicity ε_0 . As the two order parameters have the same temperature dependence, their temperature independent ratio is $\frac{\psi_0}{\varepsilon_0} = \frac{C_{66,0}}{\lambda}$. Physically, the magnitude of ε_0 is determined by the softness of the bare shear modulus $C_{66,0}$ and the strength of the nematic elastic coupling λ . As k and $\lambda/C_{66,0}$ are the proportionality constants of η_0 (resistivity anisotropy) and ε_0 (structural orthorhombicity) to the primary nematic order parameter ψ_0 , respectively, the spontaneous elastoresistivity coefficient $m_s = \frac{\eta_0}{\varepsilon_0}$ can also be considered as the ratio of the nematic coupling to the conduction electrons and to the lattice, $m_s = \frac{k}{(\lambda/C_{66,0})}$.

With this result, we now show that the spontaneous elastoresistivity coefficient can be obtained *without* measurements below the phase transition by analyzing the corresponding quantity in the disordered phase, the normal elastoresistivity coefficient $2m_{66} = \frac{d\eta}{d\varepsilon}$. The $2m_{66}$ coefficient is proportional to the nematic susceptibility $\chi_N = \frac{d\psi}{d\varepsilon}$, i.e. $2m_{66} = k\chi_N \propto (T - T^*)^{-1}$, which has a Curie-Weiss temperature dependence *above* the phase transition²⁻⁴. Interestingly, the Weiss temperature corresponds to the bare nematic transition temperature T^* , which is lower than the actual phase transition temperature T_S . As nematic fluctuations diverge towards T^* , the linear coupling to the lattice effectively softens the shear modulus to zero at T_S which induces the structural transition at this higher temperature. Thus, the crystal lattice provides a polarizable medium that enhances the nematic instability. At the transition, the nematic susceptibility attains a finite value $\chi_N(T_S) = \frac{C_{66,0}}{\lambda}$, which is exactly the same value of the ratio $\frac{\psi_0}{\varepsilon_0}$ maintained below the phase transition. Therefore, the softer the bare shear modulus $C_{66,0}$ and the stronger the nematic elastic coupling λ , the smaller the χ_N is required to satisfy the phase transition condition. From this equality of thermodynamic quantities, $\frac{\psi_0}{\varepsilon_0} = \chi_N(T_S)$, we deduce that the

equality also holds for the corresponding transport coefficients, $m_s = 2m_{66}(T_S)$, if the constant k is invariant *across* the phase transition.

In Figure 3e, we compare our measurement of m_s to $2m_{66}$ for a second sample from the same growth batch measured using the standard modified Montgomery measurement². The $2m_{66}$ data follows a Curie-Weiss fit over a range 100K-200K, with $R^2 > 0.99$. Between 80K and 100K (note the slightly higher transition temperature, $T_S = 79.5K$) the value is sub-Curie Weiss, as is commonly found for dopings near the optimal doping. We find that the measured value of 128 and the high temperature fit value of 148 of $2m_{66}(T_S)$ fall within our estimated range of m_s . The agreement between m_s and $2m_{66}(T_S)$ confirms that the proportionality of nematicity to resistivity anisotropy (k) is essentially unchanged through the phase transition, and so the resistivity anisotropy remains a valid proxy of the nematicity above, below and through the transition.

Nematic Fluctuation Softening of the Shear Modulus

Finally, we independently verify the equality $\chi_N(T_S) = \frac{C_{66,0}}{\lambda}$ by analyzing the temperature dependence of the shear modulus C_{66} , which can be extracted from the lattice response to uniaxial stress. The temperature dependence of C_{66} emerges from the second derivative of the Landau free energy with respect to strain, as $C_{66} = C_{66,0} - \lambda\chi_N$. Therefore, we expect C_{66} to also show a Curie-Weiss temperature dependence and approach zero at T_S . Figure 4a shows the inline and transverse in-plane lattice constants at 74K, just above the transition temperature. Both lattice constants show a large response to strain which is dampened with increasing applied strain. The orthorhombicity likewise has an increasingly nonlinear response to strain with cooling (Fig. 4b). We define the strain transmission as $\frac{d\varepsilon_{xx}}{d\varepsilon_{xx}^{nom}}$ and the in-plane Poisson ratio as $\nu_{xy} = -\frac{d\varepsilon_{yy}}{d\varepsilon_{xx}}$, where ε_{xx} , $\varepsilon_{yy} = \frac{\Delta L}{L_0}$ are the XRD-measured strains of the inline and transverse lattice constants, respectively. In Figure 4c, a large enhancement of strain transmission occurs with cooling, approaching 95% at T_S . The application of tensile and compressive stress

stiffens the sample and the strain transmission returns to a baseline ~40%-50% value. The Poisson ratio also shows similar behavior (Fig. 4d): under zero stress, ν_{xy} approaches 1 with cooling to T_S and decreases even faster with increasing nominal strain. All these effects can be understood in terms of the shear modulus C_{66} approaching zero at T_S and the stiffening of C_{66} as applied strain tunes the system away from the critical point.

We extract the shear modulus from the zero-stress value of the Poisson ratio using $C_{66} = (50.5 \text{ GPa}) \frac{1-\nu_{xy}}{1+\nu_{xy}}$, where the magnitude is determined from other elastic modulus terms using ultrasound data from ref.¹⁶ (see supplementary materials). In Figure 4e, we observe C_{66} diminishes to nearly zero at T_S . The Curie-Weiss fitted temperature dependence (red line) yields a fitted value of the bare shear modulus $C_{66,0} = 38.8 \pm 4.7 \text{ GPa}$ in agreement with the high-temperature ultrasound data¹⁶. The extracted $T_S - T^* = 23.8K \pm 8.3K$ agrees with the Curie-Weiss fitted value for the $2m_{66}$ data presented in Figure 3e of $T_S - T^* = 28K \pm 0.5K$; however, this is considerably smaller than the value obtained from several other shear modulus measurements^{28,29}, where $T_S - T^* \sim 40K - 50K$. Puzzlingly, a variety of such measurements have not observed the shear modulus to drop to zero at the transition as is expected. In our measurement the Poisson ratio diverges to 1 at T_S , and so our measured quantity has its largest value at the transition itself. From this result, we can conclude that the nematic susceptibility follows a Curie-Weiss temperature dependence up to the transition temperature and attains a value at T_S of $\chi_N(T_S) = \frac{C_{66,0}}{\lambda}$.

Discussion and Conclusion

We now return to the doping dependence of $2m_{66}(T_S)$ shown in Figure 1, which not only indicates that nematic fluctuations themselves are enhancing but also that the direct coupling of nematicity to conduction electrons is enhancing. Thus, even though the size of the thermodynamic order parameter vanishes as the system is tuned close to the quantum phase transition, the conduction electrons at the

Fermi surface become increasingly sensitive to the orthorhombic distortion. Such an enhancement has been inferred from previous measurements of $2m_{66}$ in the same material system^{10,30}. In this work we clearly establish the correspondence of $2m_{66}(T_S)$ to the ordered phase quantity, the spontaneous elastoresistivity coefficient m_S , and provide a direct physical explanation; **the ratio between the symmetry breaking transport coefficient and the thermodynamic order parameter enhances on approach to the critical point, suggesting that the sensitivity of conduction electrons to the lattice orthorhombicity enhances with doping even as the nematic order is suppressed.** The observation of an enhanced value of $2m_{66}(T_S)$ near the nematic quantum critical point of $\text{FeSe}_{1-x}\text{S}_x$ ³ and $\text{LaFe}_{1-x}\text{Co}_x\text{AsO}$ ⁴ indicates that this is generic to several families of iron-based superconductors.

From the experimental perspective, the use of x-ray diffraction gives unprecedented detail in the detwinning process itself and reveals a highly non-linear structural response close to the phase transition. While similar uni-axial stress approaches have been used recently to explore interesting properties in iron pnictides and beyond³¹⁻³⁷, this work highlights the importance of in-situ microscopic measurement of structurally-complex quantum materials.

Methods

Supplementary materials available upon request.

Sample Preparation: Single crystal samples of $\text{Ba}(\text{Fe}_{0.96}\text{Co}_{0.04})_2\text{As}_2$ were grown from an FeAs flux as described elsewhere³⁸. The primary sample used in x-ray measurements was prepared as a thin bar of dimensions 2.0 x 0.57 x 0.07 mm and cut along the Fe-Fe bonding direction. A piezo-actuator uniaxial strain device (*Razorbill Instruments, CS-100*) was used to provide in-situ strain. The nominal strain

(ε_{xx}^{nom}) is defined as $\frac{\Delta L}{L_0}$, where $L_0=1.08\text{mm}$ is the size of the gap between two titanium plates on which

the sample was glued with Stycast epoxy. The displacement ΔL was determined from sampling a

capacitance strain gauge using an Andeen-Hagerling AH2550A capacitance bridge. Nominal strains of $\pm 0.5\%$ were obtainable with this setup, which was sufficient to fully detwin the sample at all temperatures. The four-wire electrical contact geometry is illustrated in Figure 2a. Gold wires were glued with DuPont 4929 silver epoxy underneath the sample to not obstruct the x-ray diffraction off the top surface of the crystal. Measurements of the resistivity coefficient ρ_{xx} aligned along the stress axis were performed using a standard 4-point measurement and an SR830 lock-in amplifier. A second sample from the same batch was prepared as in ref² and the modified Montgomery method was used to determine $2m_{66}$. X-ray diffraction (XRD) measurements were performed at the Advanced Photon Source, beamline 6-ID-B, at Argonne National Laboratories. X-rays of energy 11.215 keV illuminated an area 500x500 μm , fully encompassing a cross section of the middle of the crystal where strain transmission is highest. The sample and strain device were mounted on a closed cycle cryostat. Gaussian fits to the tetragonal $(2\ 2\ 12)_T$, $(-1\ 1\ 14)_T$ and $(0\ 0\ 14)_T$ reflections were used to determine the orthorhombic lattice constants in the direction of applied stress (a_A & b_B), in-plane transverse to the stress (a_B & b_A) and normal to the plane (c), as labeled in Figure 2a.

Acknowledgments: We thank Cenke Xu, Jing-Yuan Chen, and Matthias Ikeda for discussion. **Funding:** This work was mainly supported by NSF MRSEC at UW (DMR-1719797) and the Air Force Office of Scientific Research Young Investigator Program under Grant FA9550-17-1-0217. J.H.C. acknowledge the support of the Gordon and Betty Moore Foundation's EPIQS Initiative, Grant GBMF6759 to J.-H.C, the David and Lucile Packard Foundation, the Alfred P. Sloan foundation and the State of Washington funded Clean Energy Institute. J. L. acknowledges support from the National Science Foundation under Grant No. DMR-1848269. This research used resources of the Advanced Photon Source, a U.S. Department of Energy (DOE) Office of Science User Facility operated for the DOE Office of Science by Argonne National Laboratory under Contract No. DE-AC02-06CH11357. J.J.S. was partially supported by

the U.S. Department of Energy, Office of Science, Office of Workforce Development for Teachers and Scientists, Office of Science Graduate Student Research (SCGSR) program, administered by the Oak Ridge Institute for Science and Education (ORISE) for the DOE. ORISE is managed by ORAU under contract number DE-SC0014664.

Author contributions: J.M. grew the samples. J.J.S. and P.M. did the experiments. P.R., J.-W.K., and J.L. helped conceive and design the XRD measurements at the APS. J.J.S. analyzed the data. J.H.C. supervised the project. All authors contributed extensively to the interpretation of the data and the writing of the manuscript.

Competing interests: Authors declare no competing interests.

References

1. Fradkin, E., Kivelson, S. A., Lawler, M. J., Eisenstein, J. P. & Mackenzie, A. P. Nematic Fermi Fluids in Condensed Matter Physics. *Annu. Rev. Condens. Matter Phys.* **1**, 153–178 (2010).
2. Kuo, H. H., Chu, J. H., Palmstrom, J. C., Kivelson, S. A. & Fisher, I. R. Ubiquitous signatures of nematic quantum criticality in optimally doped Fe-based superconductors. *Science*. **352**, 958–962 (2016).
3. Hosoi, S. *et al.* Nematic quantum critical point without magnetism in FeSe_{1-x}S_x superconductors. *Proc. Natl. Acad. Sci. U. S. A.* **113**, 8139–8143 (2016).
4. Hong, X. C. *et al.* Evolution of the nematic susceptibility in LaFe_{1-x}Co_xAsO. (2019).
5. In keeping with the most widely used notation, we refer to the B_{2g} symmetry of the tetragonal unit cell, while using an xy coordinate system aligned with the orthorhombic unit cell. See e.g. Shapiro, M. C., Hristov, A. T., Palmstrom, J. C., Chu, J. & Fisher, I. R. Measurement of the B_{1g} and B_{2g} components of the elastoresistivity tensor for tetragonal materials via transverse resistivity configurations. *Rev. Sci. Instrum.* **063902**, (2016).
6. Analytis, J. G. *et al.* Transport near a quantum critical point in BaFe₂(As_{1-x}P_x)₂. *Nat. Phys.* **10**, 194–197 (2014).
7. Hayes, I. M. *et al.* Scaling between magnetic field and temperature in the high-temperature superconductor BaFe₂(As_{1-x}P_x)₂. *Nat. Phys.* **12**, 916–919 (2016).
8. Tanatar, M. A. *et al.* Uniaxial-strain mechanical detwinning of CaFe₂As₂ and BaFe₂As₂ crystals: Optical and transport study. *Phys. Rev. B - Condens. Matter Mater. Phys.* **81**, 184508 (2010).
9. Tanatar, M. A. *et al.* Origin of the Resistivity Anisotropy in the Nematic Phase of FeSe. *Phys. Rev. Lett.* **117**, 127001 (2016).
10. Chu, J. In-Plane Resistivity Anisotropy in an Underdoped Iron Arsenide Superconductor. *Science*. **329**, 824–826 (2010).
11. Liu, L. *et al.* In-plane electronic anisotropy in the antiferromagnetic orthorhombic phase of isovalent-substituted Ba(Fe_{1-x}Ru_x)₂As₂. *Phys. Rev. B* **92**, 094503 (2015).
12. Ishida, S. *et al.* Anisotropy of the In-Plane Resistivity of Underdoped Ba(Fe_{1-x}Co_x)₂As₂ Superconductors Induced by Impurity Scattering in the Antiferromagnetic Orthorhombic Phase. *Phys. Rev. Lett.* **110**, 207001 (2013).
13. Blomberg, E. C. *et al.* In-plane anisotropy of electrical resistivity in strain-detwinned SrFe₂As₂. *Phys. Rev. B* **83**, 134505 (2011).
14. Fisher, I. R., Degiorgi, L. & Shen, Z. X. In-plane electronic anisotropy of underdoped ‘122’ Fe-arsenide superconductors revealed by measurements of detwinned single crystals. *Reports Prog. Phys.* **74**, 124506 (2011).
15. Böhmer, A. E. & Meingast, C. Electronic nematic susceptibility of iron-based superconductors. *Comptes Rendus Phys.* **17**, 90–112 (2016).
16. Fujii, C. *et al.* Anisotropic Grüneisen Parameter and Diverse Order Parameter Fluctuations in Iron-Based Superconductor Ba(Fe_{1-x}Co_x)₂As₂. *J. Phys. Soc. Japan* **87**, 074710 (2018).
17. Fernandes, R. M. *et al.* Effects of Nematic Fluctuations on the Elastic Properties of Iron Arsenide Superconductors. *Phys. Rev. Lett.* **105**, 157003 (2010).
18. Yang, F. *et al.* Nematic transitions in iron pnictide superconductors imaged with a quantum gas. *Nat. Phys.* 1–6 (2020). doi:10.1038/s41567-020-0826-8
19. Analytis, J. G. *et al.* Quantum oscillations in the parent pnictide BaFe₂As₂: Itinerant electrons in the reconstructed state. *Phys. Rev. B - Condens. Matter Mater. Phys.* **80**, 064507 (2009).
20. Shimojima, T. *et al.* Orbital-Dependent modifications of electronic structure across the magnetostructural transition in BaFe₂As₂. *Phys. Rev. Lett.* **104**, 057002 (2010).

21. Nakajima, M. *et al.* Unprecedented anisotropic metallic state in undoped iron arsenide BaFe₂As₂ revealed by optical spectroscopy. *Proc. Natl. Acad. Sci. U. S. A.* **108**, 12238–12242 (2011).
22. Watson, M. D. *et al.* Probing the reconstructed Fermi surface of antiferromagnetic BaFe₂As₂ in one domain. *npj Quantum Mater.* **4**, 1–9 (2019).
23. Hicks, C. W., Barber, M. E., Edkins, S. D., Brodsky, D. O. & Mackenzie, A. P. Piezoelectric-based apparatus for strain tuning. *Rev. Sci. Instrum.* **85**, 065003 (2014).
24. Kim, M. G. *et al.* Character of the structural and magnetic phase transitions in the parent and electron-doped BaFe₂As₂ compounds. *Phys. Rev. B* **83**, 134522 (2011).
25. Tanatar, M. A. *et al.* Direct imaging of the structural domains in the iron pnictides A Fe₂As₂ (A=Ca,Sr,Ba). *Phys. Rev. B - Condens. Matter Mater. Phys.* **79**, 1–4 (2009).
26. Carlson, E. W., Dahmen, K. A., Fradkin, E. & Kivelson, S. A. Hysteresis and noise from electronic nematicity in high-temperature superconductors. *Phys. Rev. Lett.* **96**, 097003 (2006).
27. A full derivation is presented in the supplementary materials
28. Yoshizawa, M. *et al.* Structural Quantum Criticality and Superconductivity in Iron-Based Superconductor Ba(Fe_{1-x}Co_x)₂As₂. *J. Phys. Soc. Japan* **81**, 024604 (2012).
29. Böhmer, A. E. *et al.* Nematic Susceptibility of Hole-Doped and Electron-Doped BaFe₂As₂ Iron-Based Superconductors from Shear Modulus Measurements. *Phys. Rev. Lett.* **112**, 047001 (2014).
30. Chu, J.-H., Kuo, H.-H., Analytis, J. G. & Fisher, I. R. Divergent Nematic Susceptibility in an Iron Arsenide Superconductor. *Science*. **337**, 710–71 (2012).
31. Schmidt, J. *et al.* Nematicity in the superconducting mixed state of strain detwinned underdoped Ba(Fe_{1-x}Co_x)₂As₂. *Phys. Rev. B* **99**, 064515 (2019).
32. Pfau, H. *et al.* Detailed band structure of twinned and detwinned BaFe₂As₂ studied with angle-resolved photoemission spectroscopy. *Phys. Rev. B* **99**, 035118 (2019).
33. Kissikov, T. *et al.* Uniaxial strain control of spin-polarization in multicomponent nematic order of BaFe₂As₂. *Nat. Commun.* **9**, 1058 (2018).
34. Zheng, X. Y., Feng, R., Ellis, D. S. & Kim, Y. J. Bulk-sensitive imaging of twin domains in La_{2-x}Sr_xCuO₄ under uniaxial pressure. *Appl. Phys. Lett.* **113**, 071906 (2018).
35. Kim, H. H. *et al.* Uniaxial pressure control of competing orders in a high-temperature superconductor. *Science*. **362**, 1040–1044 (2018).
36. Ikeda, M. S. *et al.* Symmetric and antisymmetric strain as continuous tuning parameters for electronic nematic order. *Phys. Rev. B* **98**, 1–6 (2018).
37. Malinowski, P. *et al.* Drastic suppression of superconducting T_c by anisotropic strain near a nematic quantum critical point. Preprint at <http://arxiv.org/abs/1911.03390> (2019).
38. Chu, J. H., Analytis, J. G., Kucharczyk, C. & Fisher, I. R. Determination of the phase diagram of the electron-doped superconductor Ba(Fe_{1-x}Co_x)₂As₂. *Phys. Rev. B* **79**, (2009).
39. Palmstrom, J. C. *et al.* Comparison of temperature and doping dependence of nematic susceptibility near a putative nematic quantum critical point. Preprint at <https://arxiv.org/abs/1912.07574> (2019).

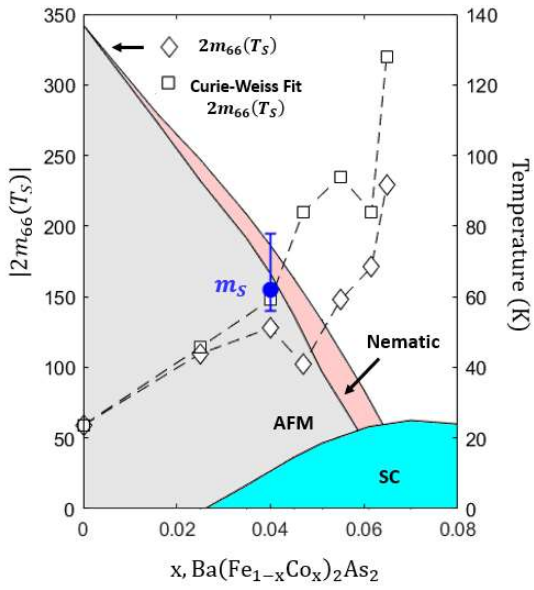


Figure 1 | x - T phase diagram of Co-doped BaFe_2As_2 . The value of the elasto-resistivity coefficient $2m_{66}$ at the nematic transition T_S shows an enhancing magnitude towards optimal doping ($x=0.067$) for both the measured value (diamonds) and for the high-temperature Curie-Weiss fit value (squares) (see Fig. 3e). The spontaneous elasto-resistivity coefficient m_S (blue) evaluated within the nematic phase is in agreement with $2m_{66}(T_S)$ values. $2m_{66}$ data for $x=0, 0.025, 0.047, 0.053$ from ref. ², for $x=0.616$ and 0.0648 from ref. ³⁹, and for $x=0.04$ from the present work.

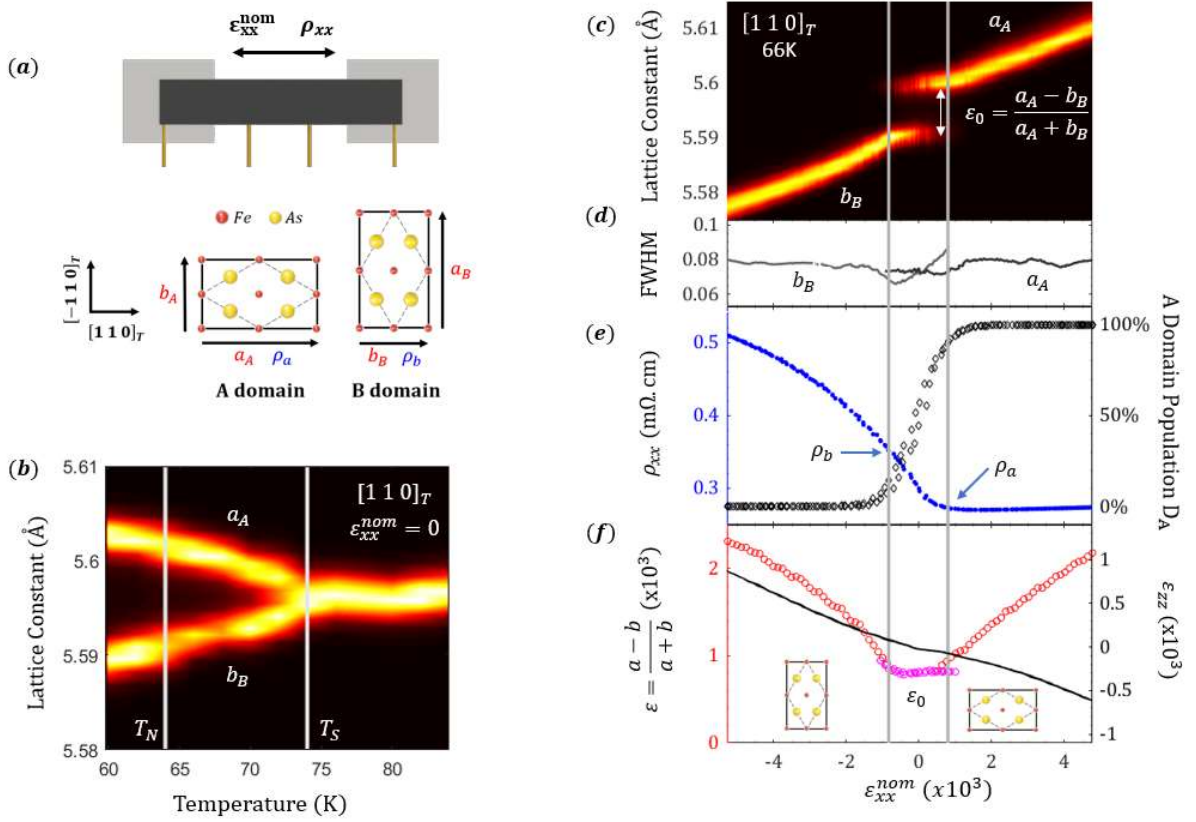


Figure 2 | X-ray diffraction of domain detwinning. (a) Schematic of the sample measurement geometry and strain device. Uniaxial stress is applied along the tetragonal $[1\ 1\ 0]_T$ direction. Inline resistivity ρ_{xx} measures ρ_a of the A domain and ρ_b of the B domain. (b) Zero-stress x-ray diffraction of the $(2\ 2\ 12)_T$ reflection yields the lattice constants aligned with the $[1\ 1\ 0]_T$ direction. (c-f) Detwinning results at 66K. (c) Nominal strain response of the $[1\ 1\ 0]_T$ direction lattice constants a_A and b_B with intensities I_A and I_B . (d) The full-width half maximum (FWHM) of the Gaussian fit to the XRD peak for both a_A and b_B . (e, right) Relative A domain population, $D_A = \frac{I_A}{I_A + I_B}$. Grey bars across figure show $D_A = 10\%$ and $D_A = 90\%$. The small spread of D_A values near zero strain is due to variance in peak intensities from strain-shifted crystal grain orientations and not due to a detwinning hysteresis (see supplementary materials). (e, left) Inline resistivity with estimates of the resistivities ρ_a and ρ_b at $D_A = 90\%$ and $D_A = 10\%$. (f, left) In-plane orthorhombicity $\varepsilon = \frac{a-b}{a+b}$ determined from within a single domain (red) or from between

the twin domains (ε_0 , magenta). (f, right) The out of plane strain $\varepsilon_{zz} = \frac{\Delta c}{c_0}$, which shows a flattened response in the detwinning strain regime.

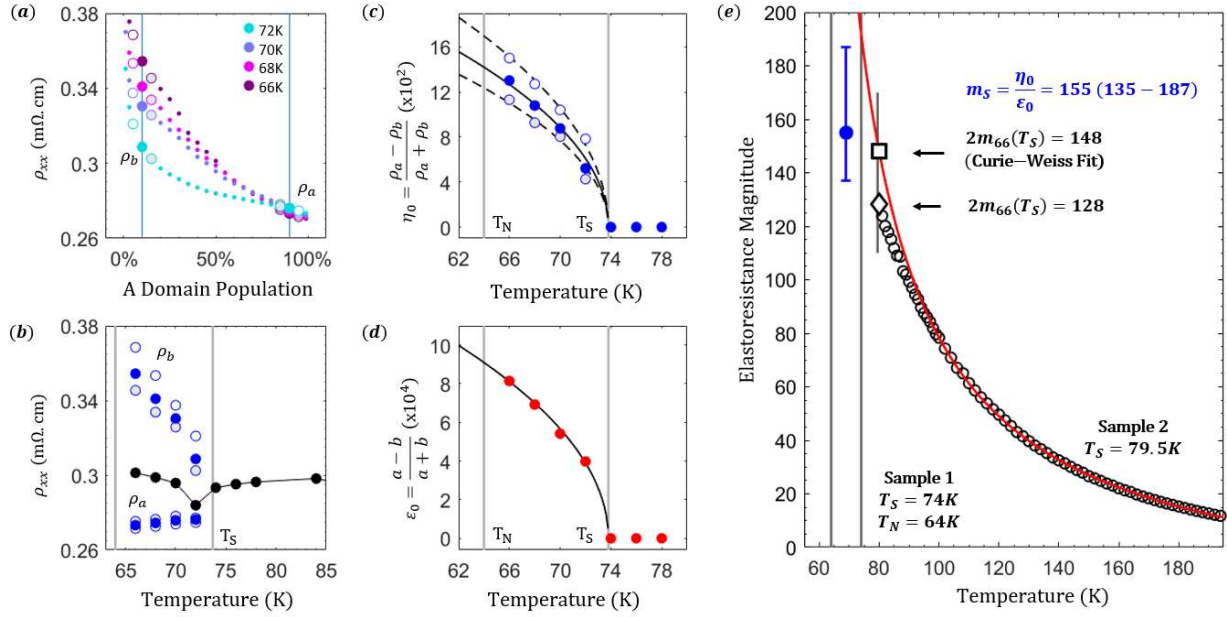


Figure 3 | Spontaneous Elastoressistivity Coefficient. (a) Resistivity ρ_{xx} as a function of A domain population at 4 temperatures within the nematic phase. The zero-stress monodomain resistivities ρ_a and ρ_b are extracted from the 10% and 90% D_A points (filled circles), with an under-over estimate taken at the 15%/85% and 5%/95% D_A points (grey/white circles). (b) The values of ρ_a and ρ_b below the transition and the measured ρ_{xx} at the zero nominal strain point (black). (c-d) The spontaneous resistivity anisotropy η_0 and the spontaneous orthorhombicity ε_0 within the nematic phase. Both quantities are well fit to a $(T_S - T)^{\frac{1}{2}}$ temperature dependence with $T_S = 73.8K$ and $R^2=0.97$ and 0.99 respectively, indicating that both are proportional to a mean-field nematic ordering. (e) The spontaneous elastoressistivity coefficient is determined from the ratio of the fits to η_0 and ε_0 as $m_S = \frac{\eta_0}{\varepsilon_0} = 155$ (135-187) (blue). The $2m_{66}$ elastoressistivity coefficient was measured for a second sample (black circles) in the disordered phase. At the second sample's nematic transition temperature, $T_S = 79.5K$, both the measured value (diamond) and high-temperature Curie-Weiss fit value (square) are within or close to the estimated range of the spontaneous elastoressistivity coefficient.

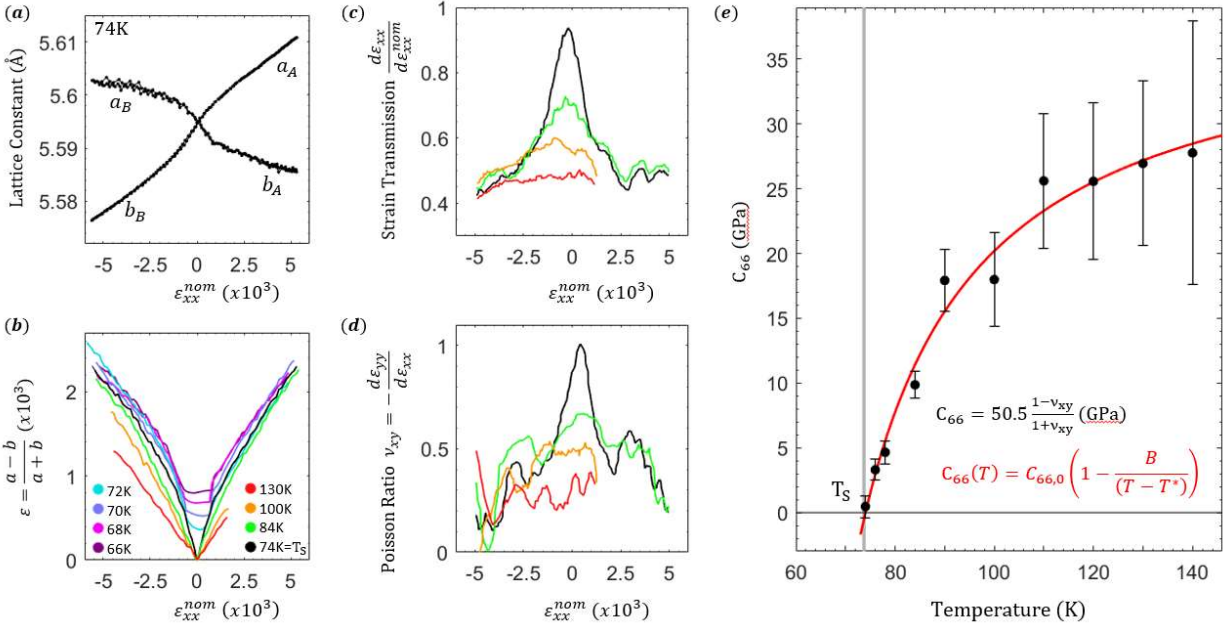


Figure 4 | Nematic fluctuation softening of the shear modulus. (a) In-plane lattice constants vs strain at $T = 74K$, concurrent with the structural transition. Within the disordered phase we refer to the strain-induced A and B domains as we do the spontaneous domains below the transition. (b) In-plane orthorhombicity vs nominal strain above and below the transition. (c) The strain transmission $\frac{d\epsilon_{xx}}{d\epsilon_{xx}^{nom}}$ and (d) in-plane Poisson ratio $\nu_{xy} = -\frac{d\epsilon_{yy}}{d\epsilon_{xx}}$ vs nominal strain. We define $\epsilon_{xx} = \frac{\Delta L}{L_0}$ as the strain of the lattice constant along the uniaxial stress direction ($[1\ 1\ 0]_T$), and likewise ϵ_{yy} for the in-plane transverse direction ($[-1\ 1\ 0]_T$). Both strain transmission and in-plane Poisson ratio show an enhancement near zero strain which increases with cooling to the transition. (e) Extracted shear modulus vs temperature. The shear modulus is determined from the peak value of the in-plane Poisson ratio ν_{xy} as $C_{66} = 50.5 \frac{1-\nu_{xy}}{1+\nu_{xy}}$ (GPa). Error bars represent one standard deviation (derived from the standard deviation of ν_{xy} over a small strain range 1.5×10^{-3} about the peak value of ν_{xy}). The shear modulus over a temperature range of 74K to 140K is well fitted to a Curie-Weiss temperature dependence as $C_{66}(T) =$

$C_{66,0} \left(1 - \frac{B}{(T-T^*)}\right)$, with $R^2 = 0.97$ and fit values $C_{66,0} = 38.8 \pm 4.7 \text{ GPa}$, $T^* = 50.0 \pm 8.3 \text{ K}$ and $B = 24.0 \pm 7.8 \text{ K}$.